# The Electro-oxidation of Hydrazine with Palladium Nanoparticle Modified Electrodes: Dissecting Chemical and Physical Effects: Catalysis, Surface Roughness or Porosity?

Ruiyang Miao, Minjun Yang, Richard G Compton*

Department of Chemistry, Physical and Theoretical Chemistry Laboratory,

University of Oxford, South Parks Road,

Oxford, OX1 3QZ, Great Britain

*Corresponding author

Email: richard.compton@chem.ox.ac.uk

Phone: +44 (0) 1865 275957 Fax: +44 (0) 1865 275410

## Abstract

Palladium nanoparticles in the form of a layer on the surface of an electrode are shown to be electro-catalytic in respect of the four-electron oxidation of hydrazine to form di-nitrogen. Quantitative voltammetry shows that the reduced over-potential in comparison with both carbon and bulk palladium electrodes partly arises from the increased surface area of the interface and partly from an increased catalytic activity of the nanoparticles relative to the bulk material. The relative catalytic activity per unit surface area of the nanoparticles as compared to the bulk material is shown to be ca. 35 - 45.


## TOC Graphic

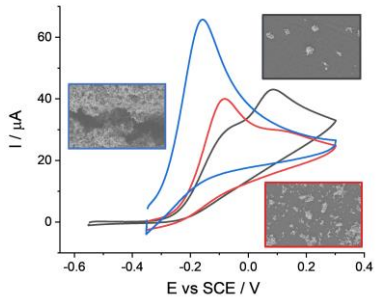


The voltammetry of hydrazine oxidation varies with the deposited coverages of palladium nanoparticles onto the glassy carbon surface, revealing the effects of both the roughness and chemically enhanced catalytic ability of palladium nanoparticles towards the reaction in comparison to bulk palladium.

The search for electro-catalysts unpins vast areas of current research in electrochemistry driven by demands for new or improved energy transformation devices and for better selective and more sensitive chemical sensors[1-4]. In both areas investigations of an extraordinarily diverse range of nano-particulate materials are ubiquitous and extensively reported as can be judged from some recent reviews[5-8]. Whilst the generation of new nano-materials is seemingly boundless as judged merely from the diversity of reported shapes - cauliflowers[9], raspberries[10], sea-urchins[11] and hollow spheres[12] - and sources of origin - metals[13], blood[14], seaweed[15], pomegranate peel[16] - as recently insightfully lampooned by Pumera *et al.*[17] - even before the diversity of chemical composition is considered. Whilst candidate electro-catalysts abound the criteria by which electro-catalysis is judged is limited, relying primarily on voltammetric methods to probe the potential at which electrochemical reactions occur on different surfaces with a lowering of over-potential indicating and measuring successful catalysis with the ultimate catalyst requiring to merely slightly exceed the thermodynamic potential for the sought (electro)chemical transformation. In practice however for many processes of interest such as the reductions of carbon dioxide, of di-oxygen, of nitrogen or the oxidation of carboxylic acids the electrochemistry is far from near reversible and improvements in electro-catalysts are simply benchmarked via lowered oxidation or reduction potentials.

It is usually implicit in voltammetric studies of electro-catalysts that the origin of a reduced over-potential is a change in the rate of the electrochemical reaction, specifically the rate of electron transfer at the solution-electrode interface. However

voltammetric half-wave potentials and peak potentials reflect not solely the heterogeneous electron transfer rate but also the prevailing mass transport conditions. Thus for example a peak potential reflects roughly the potential at which the rates of mass transport and electron transfer balance[18,19]. Consequently a change in a voltammetry can, and indeed often is, caused by a change in the rate of mass transport alone. Most familiarly this is seen in the shift observed in voltammetry of electrochemically irreversible processes between macro- and micro- electrodes with the enhanced local rates of diffusion to the latter creating a greater over-potential at electrodes made of the same material. The change simply reflects the physical size of the electrode, not the chemistry. More subtly, Kätelhön *et al*.[20] recently described the simulation of an electrode reaction at a macro-electrode which was constrained to show reversible (Nernstian) electron transfer behaviour. It was shown that if entirely inert particles showing no adsorption or electrochemistry of their own were immobilised on the surface of the electrode so altering the mass transport to the interface that voltammetric waves were obtained consistent with shifts of potential which would be consistent with either positive or negative electro-catalysis depending on the size of the spheres and the voltage scan rate despite the simulation pinning the electron transfer to be Nernstian. The shifts were related to the altered mass transport to the electrode surface as a result of the presence of the porous layers of particles and the observed responses reflected the extents to which the diffusion layer extended into or beyond the layer of particles. Clearly the voltammetry reflected physical not chemical effects despite at first sight the shifts in the voltammetric waves signalling electro-catalysis.

Similarly a simulation by Ward[21] of electrochemically irreversible processes at smooth and rough or highly porous electrodes under conditions of semi-infinite diffusion showed that a rough or porous surface could enhance the *apparent* electron transfer rate as compared to a smooth surface with a same intrinsic electrochemical rate constant by providing a greater surface area for reaction before the onset of diffusional limitations where the rate of mass transport becomes controlled by the geometric electrode area rather than the 'true' electrochemical surface area. Again this revealed a manifestation of physical not chemical catalysis.

In the present paper we explore the use of palladium nanoparticles to alter the electro-oxidation of hydrazine, $N_2H_4$, as explored voltammetrically. The reaction and its electro-catalysis are of considerable importance for fuel cells[22,23] and as a basis for chemical sensors[24,25] given the considerable toxicity of hydrazine. In particular we consider the electrochemical responses seen at glassy carbon electrodes, at bulk palladium electrodes and at palladium nanoparticle modified electrodes of both types. The addition of the palladium particles to the electrode surface is seen to markedly lower the potentials required for the oxidation which leads to the formation of di-nitrogen. We seek to identify the cause of the potential shift and ask if this is due to altered chemistry at the nanoscale, to electrode roughness, to electrode porosity or to some combination of these.

The oxidation of hydrazine was first investigated voltammetrically in 0.1 M phosphate buffer solutions (PBS) of pH 7.0 containing 1.5 mM hydrazine, at Glassy Carbon (GC) and Pd macrodisc electrodes respectively. The cyclic voltammetry was recorded as a

function of voltage scan rate. The experimental details are presented in the Supporting Information (SI) Section 1. A typical voltammogram is shown in Figure 1A for the scan rate of 50 mV/s where an electrochemically and chemically irreversible oxidative wave (solid curve) was observed at Pd macrodisc with a peak potential of ca. 0.18 V vs. SCE and a peak current of ca. 67 μA, whereas there were no voltammetric features in the absence of hydrazine (dash curve) confirming that the wave arises from the oxidation of hydrazine. At the GC surface (dot curve), an irreversible oxidative wave of hydrazine was also seen but with a peak potential of ca. 0.85 V vs. SCE and a peak current of ca. 27 μA. Evidently a much higher overpotential is required for the oxidation at the GC surface as compared to the bulk Pd surface, suggesting Pd is in comparison an effective electro-catalyst towards hydrazine oxidation. Then Tafel analysis was conducted upon the solid curve at the Pd surface so to extract the Butler-Volmer transfer coefficient. The plot of the natural logarithm of peak current lnI versus the applied potential E is displayed in the inset of Figure 1A. Note that only 10% ~ 30% of the peak current was selected for analysis to exclude the significant mass transport effect at high overpotentials.[26] The anodic transfer coefficient β was calculated to be 0.48 ± 0.01 based on the equation $\beta = Tafel\ slope \times RT/F$ , where R is the gas constant, T the temperature and F the Faraday constant. The variable scan rate data at the Pd macroelectrode was then analysed and it was found that the peak current was directly proportional to the square root of scan rate as shown in Figure 1B. This suggests the reaction be diffusion-controlled, and meanwhile the diffusion coefficient D of hydrazine was estimated to be $1.0 \times 10^{-5}$ $cm^2/s$ according to the irreversible Randles-

Ševčík equation $I_p = 2.99\times10^5 n\beta^{1/2} cAD^{1/2} v^{1/2}$, where n is the number of electrons transferred, c the analyte concentration, A the geometric area and v the scan rate. Note that hydrazine oxidation is a four-electron transfer reaction, hence n = 4 and that the first electron transfer has been assumed rate-determining[27,28].

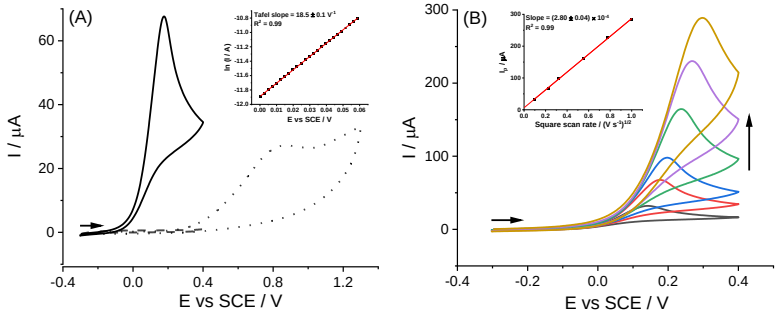


Figure 1. (A) Voltammograms in 0.1 M PBS of pH 7.0 at a scan rate of 50 mV/s: with 1.5 mM hydrazine at a Pd macrodisc electrode (solid curve), with 1.5 mM hydrazine at a GC macrodisc electrode (dot curve) and without hydrazine at a Pd macrodisc electrode (dash curve). (B) Voltammograms at the Pd macrodisc electrode in 0.1 M PBS of pH 7.0 with 1.5 mM hydrazine at variable scan rates (10/50/100/300/600/1000 mV/s). Note that the oxidative current values were obtained after baseline correction. The transverse arrows indicate the start and direction of the voltammetric scans. The vertical arrow indicates the increasing scan rates.

Having shown that bulk Palladium is electro-catalytic towards hydrazine oxidation, at least in comparison with carbon we next investigated whether this catalysis was changed at the nanoscale and work focused on the hydrazine oxidation at the GC electrode modified with variable coverages of Pd NPs in 1.5 mM hydrazine supported by 0.1 M PBS of pH 7.0. The characterisations of the drop-casted Pd nanoparticles via scanning electron microscopy (SEM) and transmission electron microscopy (TEM) are reported in the SI Section 2. The different coverage corresponded to 2/6/7/8/12/15/18 layers of nanoparticles where the number of layers is estimated by assuming that the Pd NPs are spherical with a radius of 12.4 nm (from the TEM image) and arranged in a close packed hexagonal structure. The estimation of coverage and roughness is shown

in the SI Section 3. For the higher nanoparticle coverages, as shown in Figure S1, the drop-casted layers are essentially continuous over the electrode surface and have a high degree of porosity. The corresponding voltammograms at the voltage scan rate of 50 mV/s are plotted in Figure 2A. Significant cathodic peak potential shifts are seen for Pd NP/GC (solid curves) in comparison with Pd bulk (dash curve), suggesting a possible superior catalytic ability of Pd NPs towards hydrazine oxidation, since the peak potential at bulk Pd of 0.18 V vs. SCE shifts to -0.20 V vs. SCE for the maximum coverage studied. Note that as reported above the GC surface has a negligible response at the potentials studied.

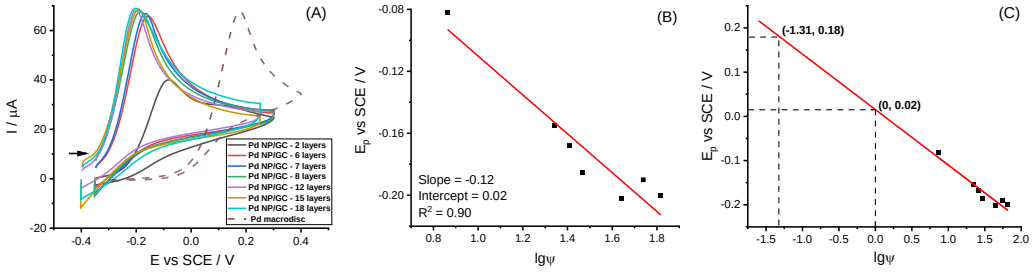


Figure 2. (A) Voltammograms at a Pd NP modified GC macrodisc electrodes with variable coverage (2/6/7/8/12/15/18, solid curves) and Pd macrodisc electrode (dash curve) in 0.1 M PBS of pH 7.0 at 50 mV/s. The transverse arrow indicates the start and direction of the voltammetric scans. (B) Plot of the peak potentials $E_p$ obtained at Pd NP modified GC macrodisc electrodes versus the logarithm of the modification coverage lgψ. (C) The extrapolation upon the fitting line in Figure 2B.

Interestingly the average baseline-corrected peak current density J calculated using the geometric area of the electrode as reported (9.22 ± 0.20 A/m$^2$) in Table 1 seen on the drop-casted electrodes is very close to that seen at Pd bulk (9.48 ± 0.07 A/m$^2$) suggesting that the voltammetric response again corresponds to that of semi-infinite diffusion with an electrochemical reaction which is overall four-electron and with the first electron transfer rate-determining. Note that the peak current data for variable

coverages shows that full coverage (from a diffusional perspective) was only realised for more than 2 layers, corresponding to the values in the table. The inference of the rate-determining step was confirmed via Tafel analysis of the voltammograms obtained for different coverages of Pd nanoparticles. The measured anodic transfer coefficients, β, are summarised in Table 1 which shows that the values are, within experimental error the same as for bulk Pd.

Table 1. Peak current density and anodic transfer coefficient of hydrazine oxidation at the bulk Pd and the Pd NP/GC of variable drop-casting coverages

| **Layers** | **6** | **7** | **8** | **12** | **15** | **18** | **Bulk** |
|---|---|---|---|---|---|---|---|
| J ($A/m^2$) | 9.12 ± 0.10 | 9.19 ± 0.09 | 9.24 ± 0.08 | 9.34 ± 0.09 | 9.19 ± 0.09 | 9.25 ± 0.11 | 9.48 ± 0.07 |
| β | 0.47 ± 0.01 | 0.48 ± 0.01 | 0.47 ± 0.01 | 0.49 ± 0.01 | 0.49 ± 0.01 | 0.49 ± 0.01 | 0.48 ± 0.01 |

Significantly the peak potentials of the voltammograms seen at the drop-casted electrode surfaces can be seen in Figure 2A to systematically move cathodically with an increase in the coverage of Pd nanoparticles leading to a value more negative than ca. -0.2 V vs. SCE for coverages in excess of 12 layers. The variation of peak potential and the essential invariance of the peak current to coverage together with the close similarity of the peak current density to the bulk Pd signal suggest that although the hydrazine oxidation reaction has reached the full electrochemically irreversible limit[21], the *effective* electrochemical rate constant of the oxidation seemingly increases with the loading of the drop-casted Pd NPs at the GC surface.

As discussed above the peak potential in a voltammogram reflects a balance between the mass transport and the rate of the electrochemical reaction. The similarity of the peak current densities as measured relative to the geometric area of the electrode

indicates that the mass transport is controlled by semi-infinite diffusion. The effective electrochemical rate constant for an electrochemically irreversible electrode reaction at a rough/porous surface has been studied by Ward *et al*.[21,29] via detailed simulation who considered both the electrochemical rate constant and the effective area of the particles forming the conductive porous layer. Ward established the following equation

$$E_p = E_f^0 + \frac{RT}{\beta F}\left[0.780 - 2.303\lg\left(\psi k^0\right) + \ln\left(\sqrt{\frac{\beta F D v}{RT}}\right)\right]$$

where $E_f^0$ is the formal potential, $k^0$ the standard electrochemical rate constant and ψ the roughness factor (ψ = total surface area of electroactive nanoparticles/substrate geometric area). The total surface area of the nanoparticles used to modify the electrode for each coverage was calculated assuming spherical particles of radius 12.4 nm (from the TEM image) and a plot of experimental $E_p$ vs. lgψ was then made and analysed as shown in Figure 2B giving a slope of -0.12 ± 0.01, from which β can be deduced to be 0.49 ± 0.03. This value is in good agreement with that extracted from the voltammogram via Tafel analysis, suggesting that the cathodic potential shift resulting from the coverage change is (at least partially) controlled by the physical surface roughness leading to an enhanced total surface area of electro-catalytic Pd. Figure 2C displays the extrapolation of the fitting line in Figure 2B, from which notably as lgψ = 0 (ψ = 1) theoretically corresponding to bulk Pd, the peak potential is ca. 0.02 V vs. SCE. This is less than the experimentally measured one (0.18 V) in Figure 2A (dash curve). The results suggest that the modification of the GC electrode with Pd nanoparticles creates a surface which is electro-catalytic towards hydrazine oxidation partly because of a surface area effect and additionally partly because the Pd

nanoparticles are more chemically catalytic than bulk Pd.

Next the standard electrochemical rate constants for the nanoparticles and for the bulk Pd were considered and the rate constant ratio $k_{Pd\ NP/GC}^{0}/k_{Pd}^{0}$ was introduced to quantitatively describe the enhanced catalytic ability from Pd NPs, in contrast to Pd bulk, on the electrochemical rate constant. Herein, $k_{Pd\ NP/GC}^{0}$ and $k_{Pd\ bulk}^{0}$ are the electrochemical rate constants of hydrazine oxidation at the Pd NP/GC and Pd macrodisc electrode respectively. Comparison of the two rate constants indicates the relative electro-catalytic activity of the two types of palladium, bulk and nano-particulate. By measuring potential variation with coverage as plotted in Figure 2B and comparing with the peak potential for bulk Pd where the electrochemical surface area is approximated by the geometrical area multiplied by a surface roughness, it is possible to estimate the ratio of $k_{Pd\ NP/GC}^{0}/k_{Pd\ bulk}^{0}$ of 43 ± 11, suggesting the electrochemical rate constant was increased by around 43 times due to differences in chemical reactivity at the nanoparticles as compared to the bulk Pd. Note that by using Ward's equation as the basis for the plot in Figure 2B the changes in area are accounted for so that the ratio of electrochemical rate constants reflects the changed chemical catalysis separate from the physical effects of the altered area. Note that the error of the ratio results from the possible surface roughness of Pd bulk ($\psi = 1.6 \pm 0.4$)[30-33]. The details in the estimation of the electrochemical rate constant ratio are given in the SI Section 4.

To further confirm the above insights we next investigated Pd electrodes modified with Pd nanoparticles where microscopy again indicated the evolution of agglomerates/aggregates of Pd nanoparticles developing on the surface with an

increased coverage of nanoparticles. Figure 3 shows that modifying a bulk Pd electrode with 6 layers of Pd NPs leads to a very similar shift of potential as seen on the GC electrode thus ruling out substrate effects and allowing a measure of the ratio $k_{Pd\ NP/Pd}^0/k_{Pd\ bulk}^0$ which was found to be 32 ± 8 in good agreement with the ratio $k_{Pd\ NP/GC}^0/k_{Pd\ bulk}^0$ determined above, where $k_{Pd\ NP/Pd}^0$ is the standard electrochemical rate constant of hydrazine oxidation at the Pd NP/Pd.

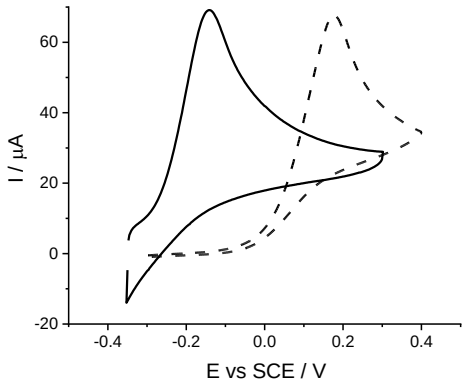


Figure 3. Voltammograms in 0.1 M PBS of pH 7.0 at the scan rate of 50 mV/s at the Pd NP modified Pd macrodisc electrode of 6 layers (solid curve) and Pd macrodisc electrode (dash curve).

Last it is interesting to look at the voltammetry of hydrazine oxidation for sparse coverages of nanoparticles. Specifically we considered 0.02, 0.1 and 0.2 layers of the Pd NP/GC. As illustrated in Figure 4, three types of peaks were observed as labelled 1, 2 and 3 where Peaks 1 and 2 emerged on the addition of increased Pd nanoparticles to the surface and Peak 3 was related to the response of the unmodified GC electrode in the absence of hydrazine (see SI Section 5). Noting that the scanning electron microscopy images in Figure S1 showed that the low coverage surfaces were comprised of individual nanoparticles or tiny agglomerates together with larger agglomerates with the latter evolving into the porous structures noted above, Peak 1, absent at very low coverages, was assigned to the response of large aggregates whilst peak 2, dominant at

very low coverages was assigned to individual Pd NPs or tiny agglomerates. It is interesting that two voltammetric peaks result from one simple modification of the (inactive) electrode surface and this further confirms the above inference that both physical and chemical effects can cause catalysis. Thus the small shift in peak potential seen relative to bulk Pd for Peak 2 confirms the chemical catalysis whereas the larger shift from Peak 1 reflects both the changed catalysis and the increased surface area of the surface agglomerates as they grow with increased coverage into the layers which can once of a sufficient size be analysed according to Ward's equation. Interpretation of the relative sizes on Peaks 1 and 2 is governed at least in principle by the overlap of the different diffusional fields of the electrochemical heterogeneous surface.[18]

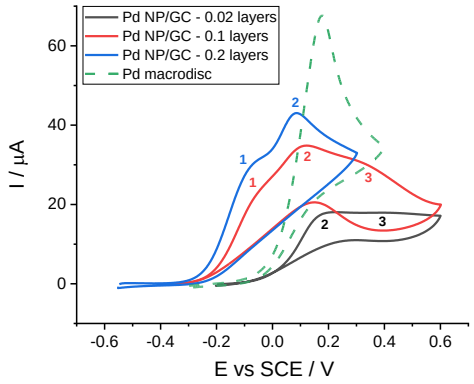


Figure 4. Voltammograms in 0.1 M PBS of pH 7.0 at 50 mV/s: (black curve) Pd NP modified GC macrodisc electrode of 0.02 layers, (red curve) Pd NP modified GC macrodisc electrode of 0.1 layers, (blue curve) Pd NP modified GC macrodisc electrode of 0.2 layers and (green curve) Pd macrodisc.

In conclusion, the catalysis of the electro-oxidation of hydrazine by palladium has been investigated both at the macro- and nano-scales. Specifically the response of layers of nanoparticles deposited on an electrode surface have been studied and the voltammetric responses analysed quantitatively. In this way it is revealed that both surface area effects and changes of chemical catalytic behaviour contribute to the reduction in over-

potential noted at the modified electrodes in comparison with bulk Palladium. The results have specific importance for the case of hydrazine and also generic significance in highlighting the essential need to dissect physical and chemical effects in electrochemical catalysis.

## Declaration of Competing Interest

The authors declare no competing interests.

## References


(1) Chia, X.; Pumera, M. Characteristics and performance of two-dimensional materials for electrocatalysis. *Nat. Catal.* **2018,** *1* (12), 909-921.

(2) Huang, Z.-F.; Song, J.; Du, Y.; Xi, S.; Dou, S.; Nsanzimana, J. M. V.; Wang, C.; Xu, Z. J.; Wang, X. Chemical and structural origin of lattice oxygen oxidation in Co–Zn oxyhydroxide oxygen evolution electrocatalysts. *Nat. Energy* **2019,** *4* (4), 329-338.

(3) Thanh, T. D.; Balamurugan, J.; Van Hien, H.; Kim, N. H.; Lee, J. H. A novel sensitive sensor for serotonin based on high-quality of AuAg nanoalloy encapsulated graphene electrocatalyst. *Biosens. Bioelectron.* **2017,** *96*, 186-193.

(4) Balasubramanian, P.; Annalakshmi, M.; Chen, S.-M.; Chen, T.-W. Ultrasensitive non-enzymatic electrochemical sensing of glucose in noninvasive samples using interconnected nanosheets-like $NiMnO_3$ as a promising electrocatalyst. *Sens. Actuators B Chem.* **2019,** *299*, 126974.

(5) Chang, Z.; Xu, J.; Zhang, X. Recent progress in electrocatalyst for Li-$O_2$ batteries. *Adv. Energy Mater.* **2017,** *7* (23), 1700875.

(6) He, J.; Manthiram, A. A review on the status and challenges of electrocatalysts in lithium-sulfur batteries. *Energy Storage Mater.* **2019,** *20*, 55-70.

(7) Alim, S.; Vejayan, J.; Yusoff, M. M.; Kafi, A. Recent uses of carbon nanotubes & gold nanoparticles in electrochemistry with application in biosensing: a review. *Biosens. Bioelectron.* **2018,** *121*, 125-136.

(8) Shrivastava, S.; Jadon, N.; Jain, R. Next-generation polymer nanocomposite-based electrochemical sensors and biosensors: A review. *Trends Analyt. Chem.* **2016,** *82*, 55-67.

(9) Wei, W.; Sun, K.; Hu, Y. H. Synthesis of 3D cauliflower-fungus-like graphene from $CO_2$ as a highly efficient counter electrode material for dye-sensitized solar cells. *J. Mater. Chem. A* **2014,** *2* (40), 16842-16846.

(10) Wang, Q.; Zheng, W.; Chen, H.; Zhang, B.; Su, D.; Cui, X. Plasmonic-induced inhibition and enhancement of the electrocatalytic activity of Pd-Au hetero-nanoraspberries for ethanol oxidation. *J. Power Sources* **2016,** *316*, 29-36.

(11) Zhang, H.; Qiu, X.; Chen, Y.; Wang, S.; Skrabalak, S. E.; Tang, Y. Shape control of monodispersed sub-5 nm Pd tetrahedrons and laciniate Pd nanourchins by maneuvering the dispersed state of additives for boosting ORR performance. *Small* **2020,** *16* (6), 1906026.

(12) Xu, F.; Tang, Z.; Huang, S.; Chen, L.; Liang, Y.; Mai, W.; Zhong, H.; Fu, R.; Wu, D. Facile synthesis of ultrahigh-surface-area hollow carbon nanospheres for enhanced adsorption and energy storage. *Nat. Commun.* **2015,** *6* (1), 1-12.
(13) Dang, S.; Zhu, Q.-L.; Xu, Q. Nanomaterials derived from metal–organic frameworks. *Nat. Rev. Mater.* **2017,** *3* (1), 1-14.
(14) Jiang, W.-J.; Hu, W.-L.; Zhang, Q.-H.; Zhao, T.-T.; Luo, H.; Zhang, X.; Gu, L.; Hu, J.-S.; Wan, L.-J. From biological enzyme to single atomic Fe–N–C electrocatalyst for efficient oxygen reduction. *Chem. Commun.* **2018,** *54* (11), 1307-1310.
(15) Liu, L.; Yang, X.; Ma, N.; Liu, H.; Xia, Y.; Chen, C.; Yang, D.; Yao, X. Scalable and cost-effective synthesis of highly efficient $Fe_2N$-based oxygen reduction catalyst derived from seaweed biomass. *Small* **2016,** *12* (10), 1295-1301.
(16) Kaviya, S.; Prasad, E. J. A. M. Sequential detection of $Fe^{3+}$ and $As^{3+}$ ions by naked eye through aggregation and disaggregation of biogenic gold nanoparticles. *Anal. Methods* **2015,** *7* (1), 168-174.
(17) Wang, L.; Sofer, Z.; Pumera, M. Will any crap we put into graphene increase its electrocatalytic effect? *ACS Nano* **2020,** *14* (1), 21-25.
(18) Compton, R. G.; Banks, C. E. Understanding Voltammetry. World Scientific: Singapore, 2018.
(19) Girault, H. H. Analytical and Physical Electrochemistry. EPFL Press: New York, 2004.
(20) Kätelhön, E.; Chen, L.; Compton, R. G. Nanoparticle electrocatalysis: unscrambling illusory inhibition and catalysis. *Appl. Mater. Today* **2019,** *15*, 139-144.
(21) Ward, K. R.; Gara, M.; Lawrence, N. S.; Hartshorne, R. S.; Compton, R. G. Nanoparticle modified electrodes can show an apparent increase in electrode kinetics due solely to altered surface geometry: The effective electrochemical rate constant for non-flat and non-uniform electrode surfaces. *J. Electroanal. Chem.* **2013,** *695*, 1-9.
(22) Rees, N. V.; Compton, R. G. Carbon-free energy: a review of ammonia-and hydrazine-based electrochemical fuel cells. *Energy Environ. Sci.* **2011,** *4* (4), 1255-1260.
(23) Serov, A.; Kwak, C. Direct hydrazine fuel cells: A review. *Appl. Catal. B* **2010,** *98* (1-2), 1-9.
(24) Deroco, P. B.; Melo, I. G.; Silva, L. S.; Eguiluz, K. I.; Salazar-Banda, G. R.; Fatibello-Filho, O. Carbon black supported Au–Pd core-shell nanoparticles within a dihexadecylphosphate film for the development of hydrazine electrochemical sensor. *Sens. Actuators B Chem.* **2018,** *256*, 535-542.
(25) Gao, F.; Wang, Q.; Gao, N.; Yang, Y.; Cai, F.; Yamane, M.; Gao, F.; Tanaka, H. Hydroxyapatite/chemically reduced graphene oxide composite: Environment-friendly synthesis and high-performance electrochemical sensing for hydrazine. *Biosens. Bioelectron.* **2017,** *97*, 238-245.
(26) Li, D.; Lin, C.; Batchelor-McAuley, C.; Chen, L.; Compton, R. G. Tafel analysis in practice. *J. Electroanal. Chem.* **2018,** *826*, 117-124.
(27) Rosca, V.; Duca, M.; de Groot, M. T.; Koper, M. T. Nitrogen cycle electrocatalysis. *Chem. Rev.* **2009,** *109* (6), 2209-2244.
(28) Miao, R.; Compton, R. G. The electro-oxidation of hydrazine: a self-inhibiting reaction. *J. Phys. Chem. Lett.* **2021,** *12* (6), 1601-1605.
(29) Ward, K. R.; Compton, R. G. Quantifying the apparent 'catalytic'effect of porous electrode surfaces. *J. Electroanal. Chem.* **2014,** *724*, 43-47.
(30) Henning, S.; Herranz, J.; Gasteiger, H. A. Bulk-palladium and palladium-on-gold electrocatalysts for the oxidation of hydrogen in alkaline electrolyte. *J. Electrochem. Soc.* **2014,** *162* (1), F178.
(31) Chierchie, T.; Mayer, C.; Lorenz, W. Structural changes of surface oxide layers on palladium. *J. Electroanal. Chem. Interf. Electrochem.* **1982,** *135* (2), 211-220.

(32) Bolzan, A.; Martins, M.; Arvia, A. The complex processes involved at Pd electrodes in 1 M $H_2SO_4$ in the potential range of oxygen electroadsorption-electrodesorption reactions. *J. Electroanal. Chem. Interf. Electrochem.* **1983,** *157* (2), 339-358.
(33) Rand, D.; Woods, R. The nature of adsorbed oxygen on rhodium, palladium and gold electrodes. *J. Electroanal. Chem. Interf. Electrochem.* **1971,** *31* (1), 29-38.